Multi-enzyme complexes on DNA scaffolds capable of substrate channeling with an artificial swinging arm

Jinglin Fu,[1, 2,#*&] *Yuhe Renee Yang,*[1,3&] *Alexander Johnson-Buck,*[4] *Minghui Liu,*[1,3] *Yan Liu,*[1,3] *Nils G. Walter,*[4*] *Neal W. Woodbury*[2,3*] *and Hao Yan*[1,3*]

[1]Center for Molecular Design and Biomimicry and [2]Center for Innovations in Medicine, Biodesign Institute at Arizona State University, Tempe, AZ 85287. [3]Department of Chemistry and Biochemistry, Arizona State University, Tempe, AZ 85287. [4]Single Molecule Analysis Group, Department of Chemistry, University of Michigan at Ann Arbor, Ann Arbor, MI 48109.

*****Corresponding author: H. Y. (hao.yan@asu.edu); J. F. (jinglin.fu@rutgers.edu); N.W.W (nwoodbury@asu.edu); N.G.W (nwalter@umich.edu)

& Equal contribution authors

Current address: Department of Chemistry, Center for Computational and Integrative Biology, Rutgers University at Camden, Camden, NJ 08102.

Swinging arms are a key functional component of multi-step catalytic transformations in many naturally occurring multi-enzyme complexes[1]. This arm is typically a prosthetic chemical group that is covalently attached to the enzyme complex via a flexible linker, allowing the direct transfer of substrate molecules between multiple active sites within the complex[2-4]. Mimicking this method of substrate channeling outside of the cellular environment requires precise control over the spatial parameters of the individual components within the assembled complex. DNA nanostructures can be used to organize functional molecules with nanoscale precision[5-7] and can also provide nanomechanical control[8-11]. Until now, protein-DNA assemblies[12] have been used to organize cascades of enzymatic reactions by controlling the relative distance and orientation of enzymatic components[13-16] or by facilitating the interface between enzymes/cofactors and electrode surfaces[17-18]. Here, we show that a DNA nanostructure can be used to create a multi-enzyme complex in which an artificial swinging arm facilitates hydride transfer between two coupled dehydrogenases. By exploiting the programmability of DNA nanostructures, key parameters including position, stoichiometry, and inter-enzyme distance can be manipulated for optimal activity.

The general design of the swinging arm nanostructure complex is shown in Fig. 1a, where a two-enzyme cascade consisting of glucose-6 phosphate dehydrogenase (G6pDH)[19] and malic dehydrogenase (MDH)[20] is displayed on a DNA double-crossover (DX) tile scaffold[21] (DNA sequences for all structures used in this study are shown in Supplementary Figs. S1-S7). G6pDH catalyzes the oxidation of glucose-6-phosphate and the reduction of NAD^+ to NADH. Subsequently, MDH catalyzes the reduction of oxaloacetate to malic acid using the NADH produced by G6pDH. To facilitate channeling of NADH between G6pDH and MDH, an NAD^+-

functionalized poly$(T)_{20}$ oligonucleotide was attached to the DNA tile surface halfway between G6pDH and MDH (see Supplementary Figs. S8-S21 for a detailed description of conjugation, assembly and purification of the nanostructured complex). Fig. 1b shows a native polyacrylamide gel electrophoresis (PAGE) analysis of the assembled enzyme complex, together with various sub-complexes. Both the gel results and the chromatogram resulting from size-exclusion chromatography (Supplementary Fig. S21) demonstrate assembly of the G6pDH-NAD^+-MDH swinging arm cascade with >80% yield. The assembled mixture was further purified by size exclusion chromatography for enzyme activity assays. Assembly of the complete complex was also visualized by atomic force microscopy (AFM) (Fig. 1c and Supplementary Fig. S57 for larger view images), where the presence of the enzymes on the structure is confirmed by differences in height ("brightness") compared to the surface of the DNA tile.

To first explore the parameters and understand the kinetics and mechanism of the restricted diffusion mediated by the ssDNA swinging arm, we developed a simplified model system (Supplementary Fig. S22). In this model, a Cy3 reporter dye takes the place of NAD^+ on the single-stranded poly$(T)_{20}$ arm, whereas a BHQ fluorescence quencher and a Cy5 energy transfer acceptor dye replace one or both enzymes on selected probe positions surrounding the swinging arm (Fig. 2a). An oligonucleotide sequence (5'-ATA GTG AAA) was extended from the 5' end of the poly$(T)_{20}$ sequence and positioned halfway between the quencher and acceptor, allowing the arm to transiently hybridize to the probes that each bear the complementary sequence (5'-TTT CAC TAT) in analogy to the binding of NAD^+/NADH to the dehydrogenases. The diffusive transport mediated by the swinging arm was then monitored by single molecule fluorescence resonance energy transfer (smFRET) between its attached reporter (Cy3) and either the quencher (BHQ, obliterating the reporter fluorescence) or the acceptor (Cy5, yielding a

distinct red fluorescence signal) using total internal reflection fluorescence microscopy as previously described[22]. Typical smFRET time traces are shown in Fig. 2a where the fluorescence signal alternates between Cy3-BHQ quenching and Cy3-Cy5 energy transfer, indicating that the poly$(T)_{20}$ arm is swinging between the two probes and transiently hybridizing to them, thus confirming its local diffusive transport. The absence of observable low-FRET intermediates (Cy3 signal only) reveals that the transient movement of the swinging arm between the two bound states occurs much more rapidly than the 100-ms time resolution of our single molecule measurements (see Supplementary Figs. S22-S25 for detailed smFRET analysis).

To characterize the distance dependence of the diffusive transport and binding mediated by the swinging arm using smFRET, we chose a design in which a single Cy5-labeled capture probe was placed at one of three topologically accessible distances from the Cy3-labeled arm: 7 nm (21 base pairs), 14 nm (42 base pairs) and 21 nm (63 base pairs). As shown in Fig. 2b, the most efficient hybridization to the capture probe was observed at 7 nm, where ~94% of all swinging arms were associated with the Cy5 probe at equilibrium (leading to high FRET). As the distance increased, the equilibrium fraction of captured swinging arms decreased to ~58% at 14 nm and only ~10% at 21 nm (Fig. 2b and Supplementary Fig. S26), due to the less efficient binding mediated by a locally tethered arm at longer distances. Furthermore, titrating in free, unlabeled ssDNA to directly compete with the swinging arm for hybridization to the capture probe allowed us to estimate the effective local concentration of the swinging arm as ~250 μM for the 7-nm design and ~2.7 μM for the 14 nm construct (Supplementary Figs. S27-28), demonstrating a steep distance dependence consistent with our predictions using a recent coarse-grained model[23] of the poly$(T)_{20}$ arm (Supplementary Fig. S29 and Table S4). Based on these

observations we predicted that our enzyme complexes would show similar distance-dependent activity.

Next, we evaluated the ability of a NAD^+-modified swinging arm to enhance dehydrogenase activity as a function of distance in complexes containing one enzyme coupled to a single NAD^+ arm (Fig. 2c and d). The activity of each of the two enzymes was measured individually in bulk solution for the three swinging arm-enzyme distances (7, 14 and 21 nm) using a phenazine methosulfat-catalyzed resazurin fluorescence assay (more details in Supplementary Figs. S30 and S33-S35)[8, 24]. As predicted, the 7-nm distance resulted in the highest activity for both G6pDH and MDH. At this distance from the NAD^+-modified swinging arm, the G6pDH-NAD^+ assembly showed an activity enhancement of ~25-fold compared to an enzyme system in the presence of the same concentration (100 nM) of freely diffusing NAD^+ (all freely diffusing NAD^+ in the main text refers to aminoethyl modified NAD^+, Supplementary Fig. S14). A spacing smaller than 7 nm is predicted to result in steric crowding between adjacent proteins and thereby reduce the assembly yield (Fig. S56). To examine possible effects of the relative orientations of the enzyme and swinging arm, we varied the angle between the NAD^+-modified arm and the enzyme attachment site while maintaining an arm-enzyme distance of ~6-8 nm (Fig. 2e and f) and found the highest activity when the arm was attached to the "top" surface of the DNA nanostructure, approximately parallel to the enzyme (Supplementary Figs. S36-S39).

Based on the evaluation of the above model systems, a G6pDH-NAD^+-MDH swinging arm structure was constructed with the NAD^+-modified arm positioned centrally, 7 nm from either enzyme in a parallel geometry. In Fig. 3a, the activity of this complete two-enzyme nanostructure is compared to that of partially assembled structures including a G6pDH-MDH assembly with freely diffusing NAD^+, a G6pDH-NAD^+ arm assembly with freely diffusing

MDH, and an MDH-NAD^+ arm assembly with freely diffusing G6pDH. For the same total NAD^+ and enzyme concentrations (100 nM each), the activity of the complete swinging arm structure is ~90-fold higher than that obtained using the same two-enzyme complex but freely diffusing NAD^+. Semi-swinging arm complexes with only one enzyme attached (G6pDH-NAD^+ or MDH-NAD^+) and the other enzyme freely diffusing in solution also resulted in somewhat higher activity than the two-enzyme complex without an NAD^+-modified arm (~14-fold for G6pDH-NAD^+, and ~4-fold for MDH-NAD^+), but were still considerably less active than the complete G6pDH-NAD^+-MDH enzyme cascade. The effective local NAD^+ concentration for G6pDH-NAD^+-MDH was determined to be ~20 μM by titrating free NAD^+ into the G6pDH-MDH assembly until the activity was equivalent to that of the G6pDH-NAD^+-MDH assembly (Fig. 3b; see Supplementary Figs. S40-S43 for detailed raw data). Notably, the effective local concentration of the NAD^+-coupled swinging arm determined by enzyme catalysis (~20 μM at 7 nm) is significantly lower than the swinging arm concentration estimated from competitive hybridization in the model system described above (~250 μM at 7 nm in Supplementary Fig. S28). We suggest that this difference may be due to the stricter orientational and sterical constraints associated with the binding of tethered NAD^+ to the active site of a nearby (anchored) enzyme. It is also possible that some enzymes or cofactors may be paired together permanently with inactive partners on the swinging arm nanostructures and hence be unable to form an active complete cascade (see more discussion below Supplementary Fig. S43). It is noticed that the effective local concentration of the single NAD^+-coupled swinging arm (~ 20 μM) is much lower than the average NAD^+ concentration in cells (~ 300 μM)[25]. However, the activity of swinging arm systems can be improved by positioning multiple NAD^+ arms around a single enzyme as

will be discussed below. The activity of swinging arms may also be constructed using more stable and active biomimetic NAD analogues in the future.

In natural multi-enzyme complexes, the relative stoichiometry of the enzymes is optimized to maximize their catalytic efficiency. Toward this end, we investigated the dependence of enzymatic activity on the number of surrounding NAD^+-modified swinging arms attached to a DNA-scaffolded 4×4 tile (Fig. 3c)[26]. For the G6pDH-NAD^+ structure, the activity increased almost linearly as the number of NAD^+-modified arms increased from 1 to 4, indicating that G6pDH activity remains well below saturation. In contrast, the enzymatic activity of the MDH-NAD^+ structure only improved twofold as the number of NAD^+-modified arms increased from 1 to 4, suggesting that MDH is approaching activity saturation (Supplementary Figs. S44-S47). Kinetic measurements of isolated enzymes indicate that G6pDH has a ~10-fold higher turnover number (k_{cat}) and an ~8-fold larger K_m than MDH (Supplementary Fig. S32), suggesting that the activity of multi-enzyme complexes might be further enhanced by increasing the ratio of MDH and NAD^+ to G6pDH. We therefore engineered structures in which two MDH molecules surround a single G6pDH molecule, channeled by two NAD^+-modified arms (G6pDH-NAD^+_2-MDH_2) as shown in Fig. 3d. As predicted, this enzyme complex exhibited an additional ~2-fold increase in activity compared to the G6pDH-NAD^+-MDH complex (Supplementary Figs. S48 and S51). Furthermore, a complex consisting of four MDH surrounding a single G6pDH channeled by four NAD^+ arms (G6pDH-NAD^+_4-MDH_4) showed ~3-fold higher activity than G6pDH-NAD^+-MDH. The performance of the G6pDH-NAD^+_4-MDH_4 complex is limited by the low yield (~50-60%) of correct assembly, possibly due to steric crowding and the complexity of the design (Supplementary Figs. S49-S51). Attesting to their

robustness, no degradation of the DNA structures was evident by PAGE analysis after 1 h of catalytic operation (Fig. S52).

Another important advantage of an enzyme cascade with a central swinging arm is the increased reaction specificity that results from restricting the diffusion of intermediates. To explore this notion, free lactate dehydrogenase (LDH) was added to compete for NADH with the malic dehydrogenase on the G6pDH-NAD^+-MDH nanostructure. The presence of LDH is expected to consume a fraction of the NADH generated by G6pDH and, thus, should interfere with the enzyme cascade, leading to decreased malic acid production (Supplementary Fig. S32). Fig. 4 shows the results of using various mixtures of enzyme complexes, containing different percentages of full G6pDH-NAD^+-MDH swinging arm in competition with free LDH for NADH. As expected, for the G6pDH-NAD^+ assembly with freely diffusing MDH and LDH we found strong competition between the two free enzymes so that the coupled activity of the G6pDH-MDH pathway was very low (Fig. 4b). As the percentage of G6pDH-NAD^+-MDH construct increased in the mixture (keeping the total enzyme concentrations constant), the MDH activity increased accordingly, indicating that the fully assembled G6pDH-NAD^+-MDH complex was effectively channeling NADH from G6pDH to MDH, avoiding competition from free LDH. LDH behaved in the opposite manner, exhibiting much lower activity as the amount of the fully assembled G6pDH-NAD^+-MDH increased (Fig. 4c). Fig. 4d presents the normalized activities of MDH and LDH against the fraction of assembled complexes.

In summary, we have designed and constructed artificial “swinging arm”-channeled multi-enzyme complexes with NAD^+-modified molecular arms to transfer hydrides between two dehydrogenase enzymes. The swinging arm not only significantly enhances enzymatic activity, but also affords high specificity in a complex environment. The concept of a flexible molecular

arm-channeled reaction should be applicable to the design and assembly of other multi-enzyme systems. For example, a similar approach can be used to construct swinging arm enzyme cascades based on other reactive cofactors such as FAD, CoA, ATP, lipoic acid, biotin or pantetheine that are used in naturally occurring multi-enzyme complexes to carry intermediates. It is also possible to engineer artificial electron-transport chains by organizing multiple redox proteins and cofactors with swinging arms, which may find utility in biofuel production and bioenergy conversion. Artificial swinging arm structures may also lead to new approaches for regulating the activity of enzymes by incorporating mechanisms for controlling the diffusion and motion of the arm. In a simple demonstration, we exchanged the ssDNA arm for a double-stranded DNA-arm (dsDNA-arm) by introducing a poly$(A)_{20}$ oligonucleotide into solution to hybridize with the NAD^+-poly$(T)_{20}$ arm. We observed a ~ 30%-50% decrease in enzyme activity for the enzyme complex with the dsDNA-arm compared to the ssDNA-arm, which Monte Carlo modeling and control experiments with poly(A) complements of varying length suggest is due to the increased structural rigidity of a completely dsDNA arm (Supplementary Fig. S53-S55). The underlying DNA nanostructure scaffolds provide programmable frameworks for creating more complex enzymatic circuitry, and may find utility in the development of functional catalytic systems for the synthesis of high-value chemicals, generation of energy, conversion of materials, and as regulatory biological circuits for diagnostic and therapeutic applications.

Acknowledgments: This work was supported by an Army Research Office MURI award W911NF-12-1-0420 to H.Y., N.G.W. and N.W.W., a National Science Foundation grant 1033222 to N.W.W. and H.Y., an Army Research Office grant W911NF-11-1-0137 to H.Y. and Y.L.. H.Y. is supported by the Presidential Strategic Initiative Fund from Arizona State

University. The authors are grateful to Jeanette Nangreave for her help in editing the manuscript, and Wei Li for his assistance with the FastScan AFM.

Author Contributions

J.F., H.Y. and N.W.W. conceived the concepts; J.F. and Y.Y. designed DNA nanostructures, performed the enzyme-DNA structure assembly and activity assay, and analyzed data; A.J. performed the smFRET experiments and analyzed date; M.L performed the 4×4 enzyme structures experiments; J.F., A.J. and Y.Y. wrote the manuscript; H.Y., N.W.W., Y.L. and N.G.W. discussed the results and commented on the manuscript.

Additional Information

This should read: Supplementary information accompanies this paper at www.nature.com/naturenanotechnology. Reprints and permission information is available online at http://npg.nature.com/reprintsandpermissions/. Correspondence and requests for materials should be addressed to H.Y., J.F., N.W.W or N.G.W.

References:

1. Perham, R.N. Swinging Arms and Swinging Domains in Multifuctional Enzymes: Catalytic Machines for Multistep Reactions. *Annu. Rev. Biochem.* **69**, 961-1004 (2000).
2. Mattevi, A. *et al.* Atomic structure of the cubic core of the pyruvate dehydrogenase multienzyme complex. *Science* **255**, 1544-1550 (1992).
3. Jitrapakdee, S. *et al.* Structure, Mechanism and Regulation of Pyruvate Carboxylase. *Biochem J.* **413**, 369-387 (2008).
4. Zhou, P., Florova, G.& Reynolds,K. A. Polyketide synthase acyl carrier protein (ACP) as a substrate and a catalyst for malonyl ACP biosynthesis. *Chem. Bio.* **6**, 577-584 (1999).
5. Seeman, N. C. Nanomaterials Based on DNA. *Annu. Rev. Biochem.* **79**, 65-87 (2010).
6. Fu, J., Liu, M., Liu, Y. & Yan, H. Spatially-interactive biomolecular networks organized by nucleic acid nanostructures. *Acc. Chem. Res.* **45**, 1215-1226 (2012).
7. Pinheiro, A. V., Han, D., Shih, W. M. & Yan, H. Challenges and opportunities for structural DNA nanotechnology. *Nature Nanotech*. **6**, 763-772 (2011).
8. Liu, M. *et al.* A DNA tweezer-actuated enzyme nanoreactor. *Nature Commun.* **4**, 2127 (2013).
9. Liedl, T., Hogberg, B., Tytell, J., Ingber, D. E. & Shih, W. M. Self-assembly of three-dimensional prestressed tensegrity structures from DNA. *Nature Nanotech*. **5**, 520-524 (2010).
10. Gu, H., Chao, J., Xiao, S.J. & Seeman, N. C. A proximity-based programmable DNA nanoscale assembly line. *Nature* **465**, 202-205 (2010).
11. Andersen, E. S. *et. al*. Self-assembly of a nanoscale DNA box with a controllable lid. *Nature* **459**, 73-76 (2009).

12. Niemeyer, C. M. Semisynthetic DNA-protein conjugates for biosensing and nanofabrication. *Angew. Chem. Int. Ed.* **49**, 1200-1216 (2010).

13. Erkelenz, M., Kuo, C.-H. & Niemeyer, C. M. DNA-Mediated Assembly of Cytochrome P450 BM3 Subdomains. *J. Am. Chem. Soc.* **133**, 16111-16118 (2011).

14. Fu, J., Liu, M., Liu, Y., Woodbury, N. W. & Yan, H. Interenzyme substrate diffusion for an enzyme cascade organized on spatially addressable DNA nanostructures. *J. Am. Chem. Soc*. **134**, 5516-5519 (2012).

15. Wilner, O. I., Weizmann, Y., Gill, R., Lioubashevski, O., Freeman, R. & Willner, I. Enzyme cascades activated on topologically programmed DNA scaffolds. *Nature Nanotech*. **4**, 249-254 (2009).

16. Delebecque, C. J., Lindner, A. B., Silver, P. A. & Aldaye, F. A. Organization of intracellular reactions with rationally designed RNA assemblies. *Science* **333**, 470-474 (2011).

17. Teller, C. & Willner, I. Organizing protein–DNA hybrids as nanostructures with programmed functionalities. *Trends Biotechnol.* **28**, 619-628 (2010).

18. Piperberg, G., Wilner, O. I., Yehezkeli, O., Tel-Vered, R. & Willner, I. Control of Bioelectrocatalytic Transformations on DNA Scaffolds. *J. Am. Chem. Soc.* **131**, 8724-8725 (2009).

19. Rowland, P., Basak, A. K., Gover, S., Levy, H. R. & Adams, H. J. The three–dimensional structure of glucose 6–phosphate dehydrogenase from Leuconostoc mesenteroides refined at 2.0 Å resolution. *Structure* **2**, 1073-1087 (1994).

20. Chapman, A. D. M., Cortés, A., Dafforn, T. R., Clarke, A. R. & Brady, R. L. Structural basis of substrate specificity in malate dehydrogenases: crystal structure of a ternary

complex of porcine cytoplasmic malate dehydrogenase, α-Ketomalonate and TetrahydroNAD. *J. Mol. Biol.* **285**, 703-712 (1999).

21. Fu, T. J. & Seeman, N. C. DNA double-crossover molecules. *Biochemistry* **32**, 3211-3220 (1993).

22. Johnson-Buck, A., Nangreave, J., Jiang, S., Yan, H.& Walter, N. G. Multifactorial Modulation of Binding and Dissociation Kinetics on Two-Dimensional DNA Nanostructure. *Nano Lett.* **13**, 2754-2759 (2013).

23. Meisburger, S. P. *et al.* Polyelectrolyte properties of single stranded DNA measured using SAXS and single molecule FRET: Beyond the wormlike chain model. *Biopolymers*, just accepted article, DOI: 10.1002/bip.22265 (2013).

24. Candeias, L. P. *et al.* The catalysed NADH reduction of resazurin to resorufin. *J. Chem. Soc., Perkin Trans. 2.* **11**, 2333-2334 (1998).

25. Yang, H. *et al.* Nutrient-Sensitive Mitochondrial NAD^+ Levels Dictate Cell Survival. *Cell* **130**, 1095–1107(2007).

26. Yan, H., Park, S. H., Finkelstein, G., Reif, J. H. & LaBean, T. H. DNA-Templated Self-Assembly of Protein Arrays and Highly Conductive Nanowires. *Science* **301**, 1882-1884 (2003).

Figure legends:

Figure 1. Design and characterization of an NAD^+-modified swinging arm providing restricted diffusion of NAD^+/NADH between two dehydrogenases. (**a**) Schematic illustration of the nanostructured complex consisting of glucose-6 phosphate dehydrogenase (G6pDH) and malic dehydrogenase (MDH) organized on a DNA DX tile. The NAD^+-modified single-stranded poly$(T)_{20}$ is positioned half-way between the two enzymes, facilitating the transfer of hydrides. (**b**) Left: Native PAGE (3%) characterization of the assembled swinging arm enzyme complex: (1) a DNA tile with the NAD^+-modified arm; (2) G6pDH-NAD^+ semi-swinging arm; (3) MDH-NAD^+ semi-swinging arm; (4) fully assembled G6pDH-NAD^+-MDH swinging arm structure. Right: fluorescence gel image of an Alexa 555-labeled G6pDH-NAD^+ structure (lane 2), an Alexa 647-labeled MDH-NAD^+ structure (lane 3), and a dual color image of a G6pDH (AlexFluor 555 labeled)-NAD^+-MDH(AlexaFluor 647 labeled) swinging arm structure (lane 4). M: double stranded DNA ladder. (**c**) AFM imaging of the G6pDH-NAD^+-MDH swinging arm structures. Scale bar: 50 nm.

Figure 2. Characterization of local diffusive transport by the poly$(T)_{20}$ swinging arm. (**a**) Single-molecule fluorescence resonance energy transfer (smFRET) characterization of the restricted diffusion of a single-stranded poly$(T)_{20}$-arm between two DNA probes anchored at either side of the structure. Top: Cy3-labeled poly$(T)_{20}$ with a 5' sticky end extension assembled between two capture probes that are modified with Cy5 (energy acceptor) and BHQ-2 (Black Hole Quencher®), respectively, with ~ 7 nm distance from the anchor position of the arm. The Cy3-Cy5 FRET signal (red emission) is observed when the arm swings and binds to the Cy5-labeled capture probe, while a Cy3-BHQ interaction quenches the fluorescence when the arm

swings and binds to the BHQ-labeled capture probe. Bottom: smFRET monitoring the swinging poly$(T)_{20}$ arm with alternating Cy3-BHQ quenching and Cy3-Cy5 FRET events. CCD integration time: 0.1 s. (**b**) smFRET characterization of the distance-dependent hybridization of the poly$(T)_{20}$ arm, with 7 nm (top), 14 nm (middle) and 21 nm (bottom) enzyme-NAD-modified arm distances. (**c & d**) Distance dependent enzyme activity for complexes in which the NAD^+-modified arm is coupled to either G6pDH (C) or MDH (D) with enzyme-NAD^+-modified arm distances of 7-nm, 14-nm and 21-nm. (**e & f**) Orientation dependent enzyme activity for complexes in which the NAD^+-modified arm is coupled to either G6pDH (E) or MDH (F) at various angles between the enzyme and arm attachment sites on the DNA scaffold. Angles of parallel or ~0˚ (T), left or ~90˚ (L), right or ~90˚(R) and bottom or ~180˚ (B) were investigated. Error bar is the generated by the value range of at least three replicates.

Figure 3. Characterization of enzymatic activity in the G6pDH-NAD^+-MDH swinging arm structures. (**a**) Normalized overall pathway activities for G6pDH-MDH assembly with free NAD^+ (G-M + NAD), G6pDH-NAD^+ semi-swinging arm with free MDH (G-NAD + M), MDH-NAD^+ semi-swinging arm with free G6pDH (NAD-M + G) and the fully assembled G6pDH-NAD^+-MDH swinging arm structure (G-NAD-M). Total enzyme structure and NAD^+ concentrations: each 100 nM. Substrate conditions: 1 mM glucose-6 phosphate and 1 mM oxaloacetic acid in 100 mM HEPES buffer (pH 8). (**b**) Titrating the effective concentration of freely diffusing NAD^+ into the G-M assembly with equivalent activity to the swinging arm structure of G-NAD-M assembly: 100 nM G-M assemblies with free aminoethyl modified NAD^+ (AE-NAD) at 2.5, 5, 10, 20 and 40 μM. All NAD^+ used in the assay refers to aminoethyl modified NAD^+. (**c**) Relative stoichiometric dependence of enzyme activity as the number of

NAD^+-modified arms on a 4 × 4 DNA tile increases from 1 to 4. (**d**) Improving the catalytic efficiency by adjusting the relative number of G6pDH and MDH molecules: G6pDH-MDH assembly with free NAD^+ (G-M + NAD); G6pDH-NAD^+-MDH swinging arm structure (G-NAD-M); G6pDH-NAD_2^+-MDH_2 swinging arm structure (G-NAD_2-M_2) and G6pDH-NAD_4^+-MDH_4 structure (G-NAD_4-M_4). Error bar is the generated by the value range of at least three replicates.

Figure 4. Specificity of the G6pDH-NAD^+-MDH swinging arm structure when free LDH is introduced to compete for the NADH produced by G6pDH. (**a**) Schematic illustration of the competition of free LDH with free MDH for the G6pDH-NAD^+ semi-swinging arm (left) and of free LDH with the fully assembled G6pDH-NAD^+-MDH swinging arm complex (right). (**b**) The dependence of MDH activity on the fraction of fully assembled swinging arm complex (SW). (**c**) The dependence of LDH activity on the fraction of fully assembled swinging arm complex. (**d**) Normalized LDH and MDH activities as a function of the fraction of assembled swinging arm complex. Assay conditions: 100 nM G6pDH-NAD^+-MDH structure (total concentration including the half and fully assembled swinging arm structures); 100 nM LDH; 1 mM glucose-6 phosphate, 1 mM oxaloacetic acid, 1 mM sodium pyruvate in 100 mM HEPES buffer (pH 8). Error bar is the generated by the value range of at least three replicates.

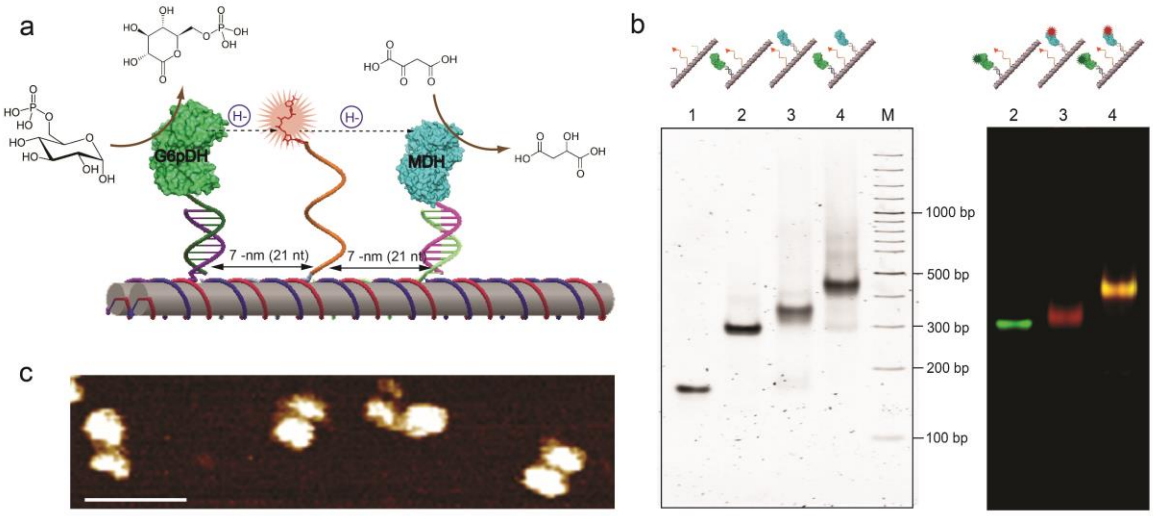
a
G6pDH
MDH
7 -nm (21 nt)
7 -nm (21 nt)
b
1
2
3
4
M
1000 bp
500 bp
300 bp
200 bp
100 bp
2
3
4
c

Figure 1

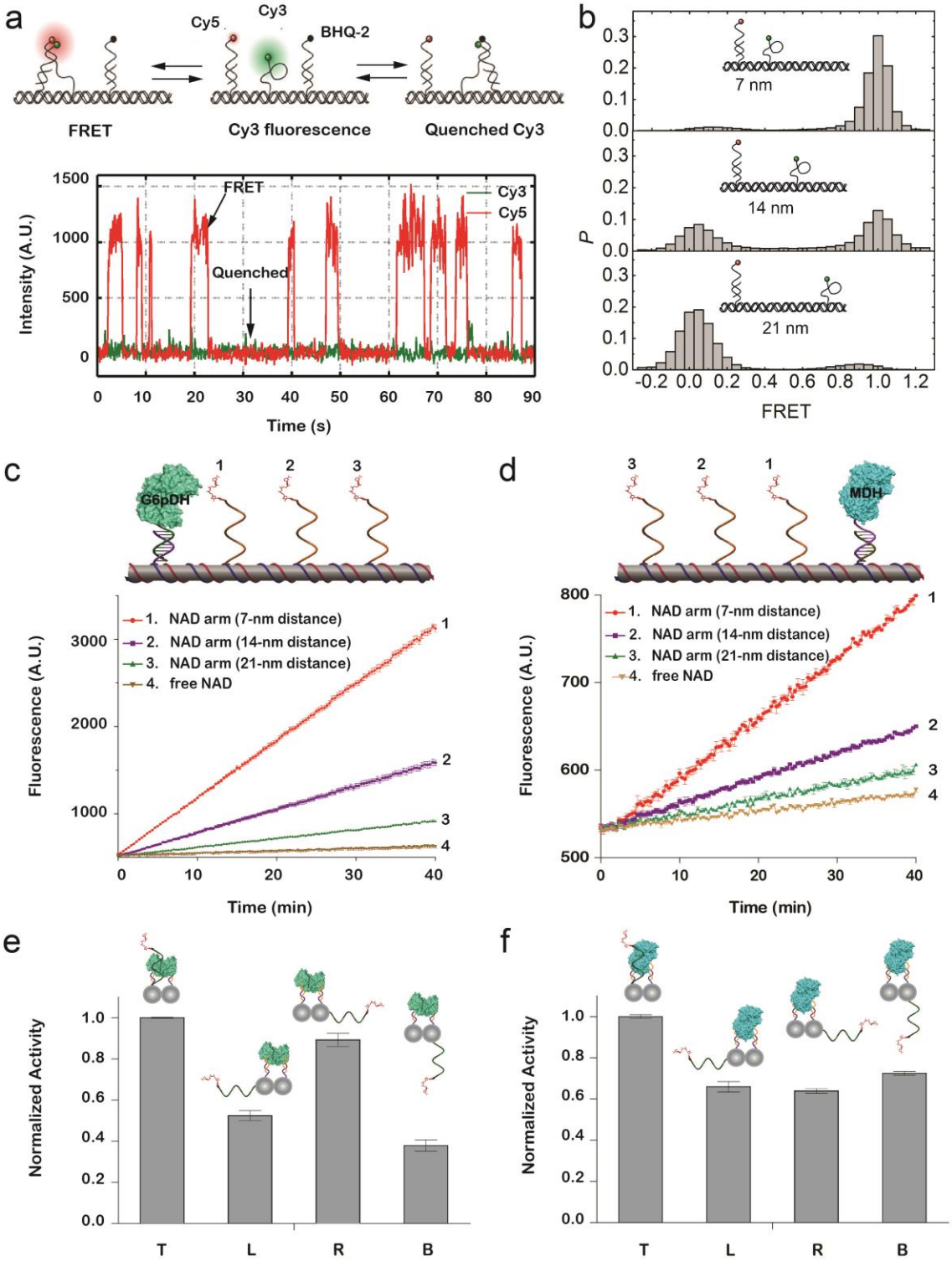
a
Cy5
Cy3
BHQ-2
FRET
Cy3 fluorescence
Quenched Cy3
Intensity (A.U.)
FRET
Quenched
Cy3
Cy5
Time (s)
b
7 nm
14 nm
21 nm
P
FRET
c
G6pDH
1
2
3
1. NAD arm (7-nm distance)
2. NAD arm (14-nm distance)
3. NAD arm (21-nm distance)
4. free NAD
Fluorescence (A.U.)
Time (min)
d
MDH
1. NAD arm (7-nm distance)
2. NAD arm (14-nm distance)
3. NAD arm (21-nm distance)
4. free NAD
Fluorescence (A.U.)
Time (min)
e
Normalized Activity
T
L
R
B
f
Normalized Activity
T
L
R
B

Figure 2

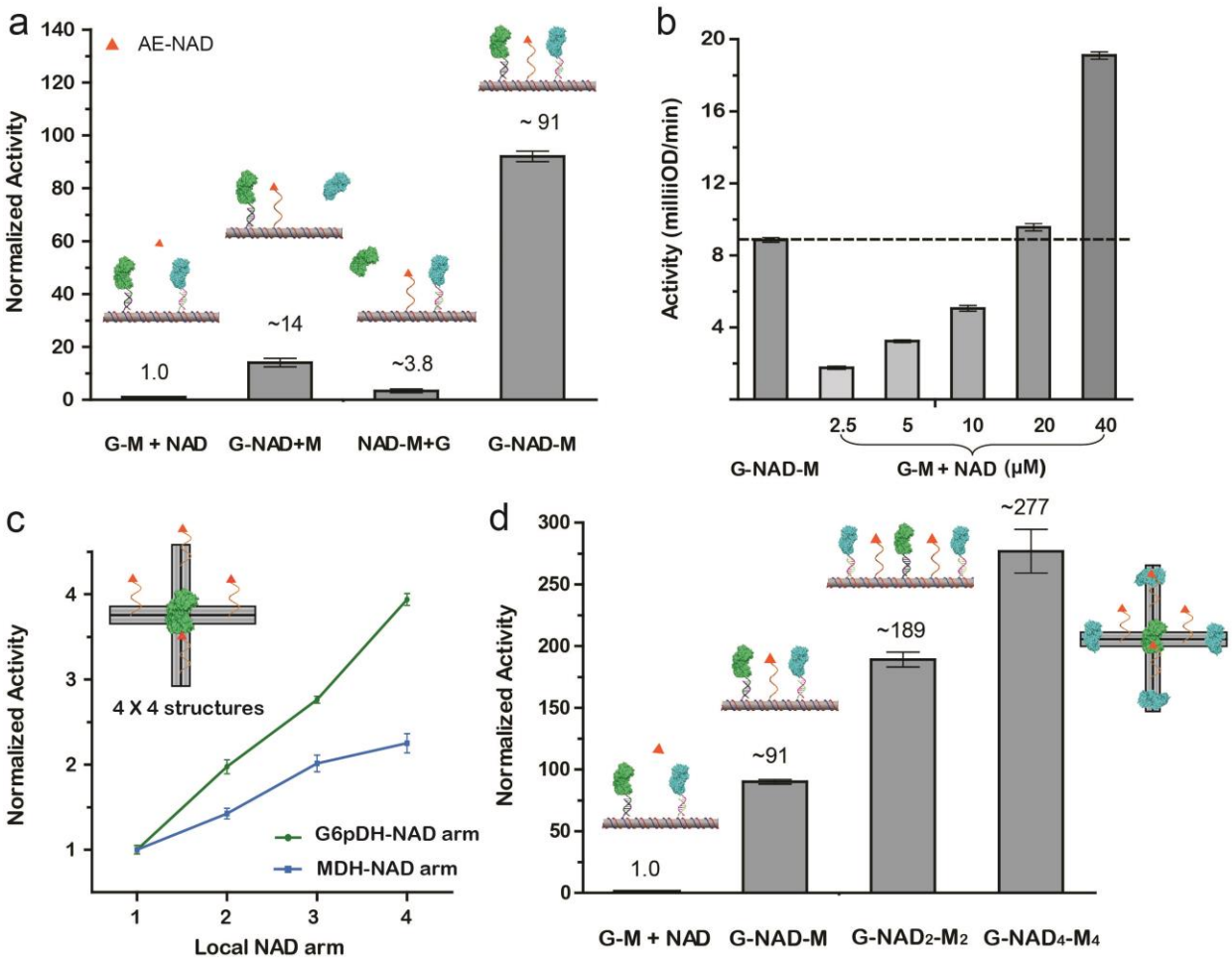
a
AE-NAD
Normalized Activity
140
120
100
80
60
40
20
0
~ 91
~14
~3.8
1.0
G-M + NAD
G-NAD+M
NAD-M+G
G-NAD-M
b
Activity (milliiOD/min)
20
16
12
8
4
2.5
5
10
20
40
G-NAD-M
G-M + NAD (μM)
c
Normalized Activity
4 X 4 structures
G6pDH-NAD arm
MDH-NAD arm
Local NAD arm
d
Normalized Activity
300
250
200
150
100
50
0
~277
~189
~91
1.0
G-M + NAD
G-NAD-M
G-NAD2-M2
G-NAD4-M4

Figure 3

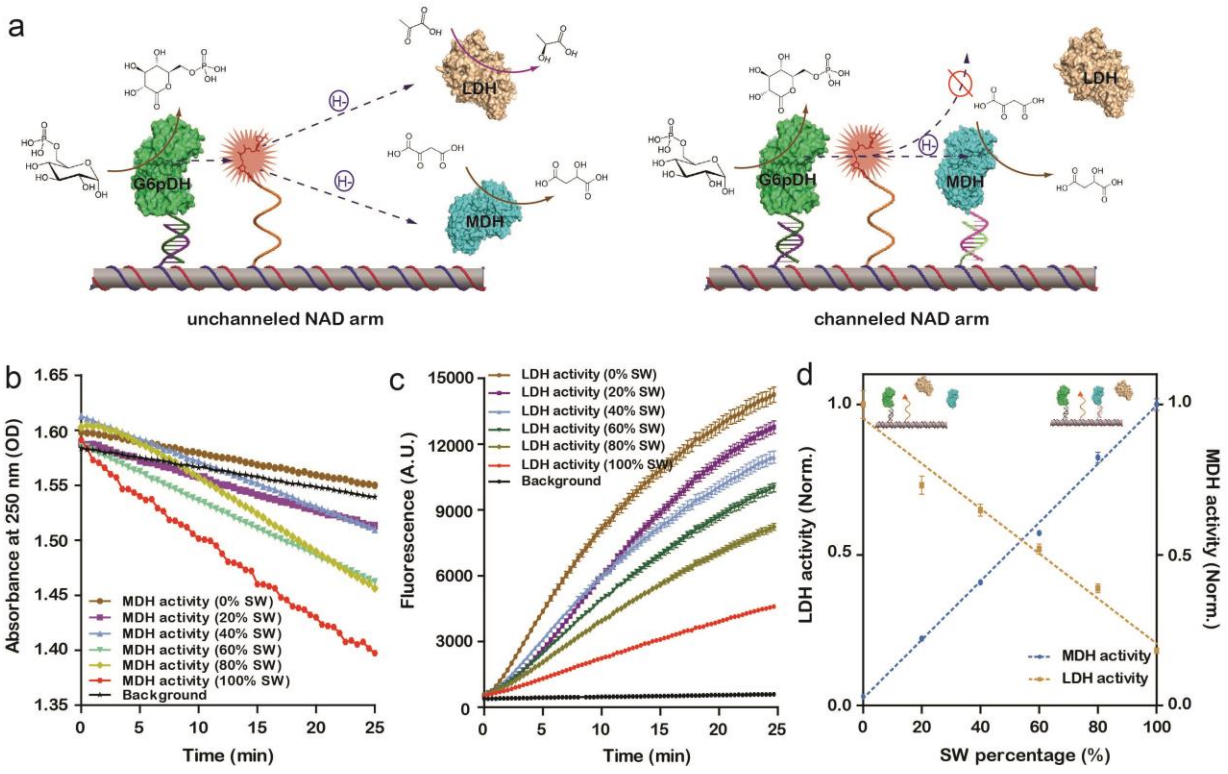
a
G6pDH
LDH
MDH
unchanneled NAD arm
channeled NAD arm
b
Absorbance at 250 nm (OD)
Time (min)
MDH activity (0% SW)
MDH activity (20% SW)
MDH activity (40% SW)
MDH activity (60% SW)
MDH activity (80% SW)
MDH activity (100% SW)
Background
c
Fluorescence (A.U.)
Time (min)
LDH activity (0% SW)
LDH activity (20% SW)
LDH activity (40% SW)
LDH activity (60% SW)
LDH activity (80% SW)
LDH activity (100% SW)
Background
d
LDH activity (Norm.)
MDH activity (Norm.)
SW percentage (%)
MDH activity
LDH activity

Figure 4